Wind and Structures, Vol. 5, No. 2~4 (2002) 277-290
DOI: http://dx.doi.org/10.12989/was.2002.5.2_4.277

Aeroelastic stability analysis of a bridge deck with added vanes using a discrete vortex method

I. Taylor†

Department of Mechanical Engineering, University of Strathclyde, Glasgow, G11XJ, Scotland, UK

M. Vezza‡

Department of Aerospace Engineering, University of Glasgow, Glasgow, G12 8QQ, Scotland, UK

Abstract. A two dimensional discrete vortex method (DIVEX) has been developed at the Department of Aerospace Engineering, University of Glasgow, to predict unsteady and incompressible flow fields around closed bodies. The basis of the method is the discretisation of the vorticity field, rather than the velocity field, into a series of vortex particles that are free to move in the flow field that the particles collectively induce. This paper gives a brief description of the numerical implementation of DIVEX and presents the results of calculations on a recent suspension bridge deck section. The results from both the static and flutter analysis of the main deck in isolation are in good agreement with experimental data. A brief study of the effect of flow control vanes on the aeroelastic stability of the bridge is also presented and the results confirm previous analytical and experimental studies. The aeroelastic study is carried out firstly using aerodynamic derivatives extracted from the DIVEX simulations. These results are then assessed further by presenting results from full time-dependent aeroelastic solutions for the original deck and one of the vane cases. In general, the results show good qualitative and quantitative agreement with results from experimental data and demonstrate that DIVEX is a useful design tool in the field of wind engineering.

Key words: computational wind engineering; discrete vortex method; bridge aerodynamics flow control; flutter; aerodynamic derivatives.

1. Introduction

As modern suspension bridge designs span ever longer distances, the necessity for more lightweight materials and the increased flexibility of the structure place challenging demands on the engineer. Aeroelastic phenomena such as vortex induced vibration, galloping and flutter, arising from the response of the structure to the unsteady aerodynamic loading have a much greater impact on the design. The catastrophic failure of the original Tacoma Narrows bridge in 1940 is a famous example of the importance of the fluid-structure interaction as a result of the loading induced by the unsteady aerodynamics (Billah and Scanlan 1991). Since the Tacoma incident, the analysis of unsteady aerodynamics and its effect on the aeroelastic response of suspension bridges has become a major topic of research. As a result, the understanding and analysis of the aerodynamic loading

† Lecturer
‡ Senior Lecturer

has advanced rapidly and techniques for predicting the onset of flutter instabilities have been established for many years (Scanlan *et al*. 1971, 1992 and 1997). Much of this analysis, however, is based on experimental investigations of the unsteady aerodynamics from wind tunnel tests of either sectional or full aeroelastic models of the structure.

For the structural analysis of bridges, the development of computational finite element models have enabled designers to experiment with a range of structural configurations and systems without the need to resort to expensive and time consuming physical testing. However, despite the rapid advances in computational hardware and the development of many numerical models in recent years, the development and application of aerodynamic models for the analysis of bridges has lagged far behind that of structural models. For this reason, much of the analysis of the aerodynamic loading and aeroelastic response of bridges is still obtained from experimental testing. However, accurate prediction of the flow field for such problems using computational methods is becoming increasingly important, to help improve the understanding of fluid-structure interactions in bluff body flows, due to the financial cost and time involved in performing wind tunnel tests. Although this presents a challenge to computational methods, recent developments in both software and hardware have been providing valuable insights.

The use of vanes to modify the aeroelastic behaviour of bridge decks has received some attention in recent times. On bluff cross-sections, the use of fairings has been shown to improve aeroelastic stability (Huston *et al*. 1988, Nagao *et al*. 1993). For streamlined sections, such as the Great Belt East main span, it has been suggested that the critical flutter velocity may be increased by the addition of guide vanes (Cobo Del Arco *et al*. 1997, Kobayashi and Nagaoka 1992). More recent control studies on decks with different flap configurations have also been made (Kwon and Chang 1999, Omenzetter *et al*. 1999). To date these studies have mainly employed simplified aerodynamic models in the simulations, for example methods based on Theodorsen's theory. This approach imposes limitations on the flow regime which can be modelled, that is bodies exhibiting trailing edge separation under low amplitude oscillatory conditions. Hence non-linear, amplitude dependent aerodynamic effects are omitted.

The discrete vortex method is a numerical technique that has undergone significant development in recent years and has been shown to be well suited to analysing unsteady and highly separated flow fields. Comprehensive reviews of the discrete vortex method are given in Sarpkaya (1989), Leonard (1980) and Puckett (1993). Vortex methods are based on the discretisation of the vorticity field rather than the velocity field, into a series of vortex particles. These particles are of finite core size, each carrying a certain amount of circulation, and are tracked throughout the flow field that they collectively induce. As a result of this approach, the model does not require a calculation mesh and provides a very different method of analysis to more traditional grid based computational fluid dynamics methods. One of the main advantages that vortex methods have, is that the Lagrangian nature of the method significantly reduces some of the problems that are associated with grid based methods. These primarily include numerical diffusion and difficulties in achieving resolution of small scale vortical structures in the flow. Vortex particles are naturally concentrated into areas of non-zero vorticity and enable vortex methods to capture these small scale flow structures in more detail. Dispensing with a calculation mesh also eases the task of modelling a more arbitrary range of geometries and in particular, vortex methods are well suited to the analysis of moving body problems.

This paper presents a two dimensional discrete vortex method (DIVEX) that has been developed at the Department of Aerospace Engineering, University of Glasgow. The model was originally developed to analyse the dynamic stall phenomena on aerofoils undergoing a pitching motion (Lin *et al*. 1996 and 1997a,b). DIVEX has recently been further developed and validated for the analysis of a range of bluff body flow fields (Taylor *et al*. 1998 and 1999).

The results presented herein are from an analysis of the Great Belt East suspension bridge (Larsen *et al.* 1992 and 1993). This bridge, opened in June 1998, has a main span of 1624 m and has been one of the major recent projects in the fields of suspension bridge aerodynamics and wind engineering. As a result, it has been the subject of numerous studies, both experimental and numerical, giving a significant database which can be used to assess the predictions from DIVEX.

DIVEX can be used purely as an aerodynamic tool or in full aeroelastic mode. In the former case both static and moving body problems can be modelled. The application of flow control devices, both passive and active, are briefly studied. The results successfully demonstrate the expected variation in the critical flutter velocity for varying configurations of flow control devices and are in good agreement with previous experimental and analytical studies.

2. Discrete vortex method

2.1. Mathematical formulation

Two dimensional incompressible viscous flow is governed by the vorticity-stream function form of the continuity and Navier-Stokes Eqs. (1) and (2) :

Continuity equation :

$$\nabla^2 \Psi = -\omega \tag{1}$$

Vorticity transport equation :

$$\frac{\partial \vec{\boldsymbol{\omega}}}{\partial t} + (\vec{\boldsymbol{U}}.\nabla)\vec{\boldsymbol{\omega}} = \nu \nabla^2 \vec{\boldsymbol{\omega}} \tag{2}$$

where the vorticity, $\vec{\boldsymbol{\omega}}$, is defined as the curl of the velocity, Eq. (3) and $\vec{\boldsymbol{\Psi}}$ is a vector potential defined by Eq. (4)

$$\vec{\boldsymbol{\omega}} = \nabla \times \vec{\boldsymbol{U}} \quad \text{with} \quad \vec{\boldsymbol{\omega}} = \vec{\boldsymbol{k}}\omega \tag{3}$$

$$\vec{\boldsymbol{U}} = \nabla \times \vec{\boldsymbol{\Psi}}, \quad \nabla.\vec{\boldsymbol{\Psi}} = 0, \quad \text{and} \quad \vec{\boldsymbol{\Psi}} = \vec{\boldsymbol{k}}\Psi \tag{4}$$

The vorticity transport Eq. (2) defines the motion of vorticity in the flow due to convection and diffusion. As the pressure field is not explicitly defined in Eq. (2), the variation of vorticity at a point in the flow is therefore influenced by the surrounding velocity and vorticity of the flow.

The calculations are subject to the far field boundary conditions, Eq. (5), and the no-slip and no-penetration conditions at the surface of the body Eq. (6).

$$\vec{\boldsymbol{U}} = \vec{\boldsymbol{U}}_\infty \quad \text{or} \quad \nabla\Psi = \nabla\Psi_\infty \quad \text{on} \quad S_\infty \tag{5}$$

$$\vec{\boldsymbol{U}} = \vec{\boldsymbol{U}}_i \quad \text{or} \quad \nabla\Psi = \nabla\Psi_i \quad \text{on} \quad S_i \tag{6}$$

The boundary conditions normal and tangential to the body surface cannot both be applied explicitly as only one component can be specified. Only the normal component (no-penetration) is satisfied explicitly although the tangential component (no-slip) is implicitly satisfied due to the representation of the internal kinematics of each solid body. The velocity at a point $\vec{\boldsymbol{r}}$ on the surface or within body i can be described by

$$\vec{\boldsymbol{U}}_i = \vec{\boldsymbol{U}}_{ic} + \vec{\boldsymbol{\Omega}}_i \times (\vec{\boldsymbol{r}}_p - \vec{\boldsymbol{r}}_{ic}) \tag{7}$$

where $\vec{\boldsymbol{r}}_{ic}$ is a fixed reference point on the body. This may also be represented in stream function form

$$\nabla^2 \Psi_i = -2\Omega_i \qquad \text{in } B_i \tag{8}$$

The relationship between the velocity and the vorticity is obtained through the application of Green's theorem to Eq. (1) for the flow region F and Eq. (8) for the body region B_i , and combining them through the boundary conditions, Eqs. (5) and (6) (Lin 1997b). From this, the velocity field is calculated using the Biot-Savart law, which expresses the velocity in terms of the vorticity field. For a point p outside the solid region, the velocity is given by :

$$\vec{\boldsymbol{U}}_p = \vec{\boldsymbol{U}}_\infty + \frac{1}{2\pi} \int_F \omega \frac{\vec{\boldsymbol{k}} \times (\vec{\boldsymbol{r}}_p - \vec{\boldsymbol{r}})}{\|\vec{\boldsymbol{r}}_p - \vec{\boldsymbol{r}}\|^2} dF + \int_{B_i} 2\Omega_i \frac{\vec{\boldsymbol{k}} \times (\vec{\boldsymbol{r}}_p - \vec{\boldsymbol{r}})}{\|\vec{\boldsymbol{r}}_p - \vec{\boldsymbol{r}}\|^2} dB_i \tag{9}$$

The pressure distribution on the body surface can be evaluated by integrating the pressure gradient along the body contour. The pressure gradient at node j on the body surface is:

$$\frac{1}{\rho}\frac{\partial P}{\partial s} = -\vec{\boldsymbol{s}}.\frac{D\vec{\boldsymbol{U}}_c}{Dt} - \vec{\boldsymbol{n}}.(\vec{\boldsymbol{r}} - \vec{\boldsymbol{r}}_c)\frac{D\Omega}{Dt} + \vec{\boldsymbol{s}}.(\vec{\boldsymbol{r}} - \vec{\boldsymbol{r}}_c)\Omega^2 + \nu\frac{\partial \omega}{\partial n} \tag{10}$$

The first three terms on the RHS are due to the body motion and represent the surface tangential components of the body reference point acceleration, the rotational acceleration and the centripetal acceleration. The final term is the negative rate of vorticity creation at the body surface and is calculated from the vorticity distribution created in the control zone between time t-Δt and t (Lin 1997b and Spalart 1988). The resulting pressure distribution is integrated around the body surface to calculate the aerodynamic forces on the body and the moment about the body reference point.

2.2. Numerical implementation

The numerical implementation of the governing equations is presented in more detail in Lin *et al*. (1996 and 1997a, b) and Taylor (1999) with only a brief summary presented here. The governing equations defined in the previous section are for most practical cases impossible to solve analytically. For this reason, an approximate solution may be obtained numerically through the discretisation of the vorticity field into a series of vortex particles. As the vorticity in the flow originates on the body surface, the discretisation of the vorticity near to the body is important so that its subsequent evolution is well captured. The idea that the vorticity is created in a thin layer around the body surface indicates that the flow can be divided into two zones. The first is the control zone near the body surface in which vorticity is created, and the second is the wake zone which contains the remaining vorticity that is shed from the body surface through convection and diffusion. These two sub-regions of the flow utilise different discretisation procedures.

For a two dimensional body, a polygonal representation of the body surface is created by connecting a series of N nodes with straight lines forming a series of panels. Each panel is further subdivided into K equal length sub-panels. The implementation of the no-penetration boundary condition on each panel enables the surface circulation density, γ, to be calculated at each body node. The γ distribution is further broken down into vortex blobs, one for each sub-panel, with the centre of the blob positioned a distance δ above the middle of the sub-panel. The spacing of the blobs is designed to ensure overlapping cores, a condition required for accurate computations with vortices (see for example Perlman 1985), and the height is of the order of the core radius.

These vortices are released from the body into the wake, where their positions are determined from convection and diffusion at each time step. The simulation of vortex convection and diffusion employs an operator splitting technique, where the vorticity transport Eq. (2) is split into a separate convection part Eq. (11) and diffusion part Eq. (12), both of which are solved sequentially as proposed by Chorin (1973).

$$\frac{\partial \omega}{\partial t} + (\vec{\boldsymbol{U}}.\nabla)\omega = 0 \tag{11}$$

$$\frac{\partial \omega}{\partial t} = \nu \nabla^2 \omega \tag{12}$$

As vorticity forms one of the conserved properties of the particles in inviscid flows, the velocity at the centre of each vortex particle is equal to the velocity of the vorticity transport which is evaluated from (9). The diffusion process is modelled using a random walk procedure (Chorin 1973) which satisfies the Gaussian distribution of zero mean and standard deviation $\sqrt{(2\nu\Delta t)}$ or in non-dimensional form $\sqrt{(2\Delta t/Re)}$, where Δt is the timestep and Re is the Reynolds number of the flow.

The calculation of the velocity of a single vortex particle requires the influence of all regions of vorticity in the flow field to be taken into account Eq. (9). For a flow field containing N particles this leads to an operation count of $O(N^2)$, which becomes prohibitive as N increases. A fast algorithm for the velocity calculation has been included in DIVEX. The procedure uses a zonal decomposition algorithm for the velocity summation and allows the effect of groups of particles on the velocity to be calculated using a single series expansion, thus significantly reducing the operation count of the calculation. The algorithm utilises a hierarchical technique similar in nature to the adaptive Fast Multipole Method (Carrier *et al.* 1988), so that the largest possible group of particles is used for each series expansion. The resulting operation count is $O(N+N\log N)$, and therefore offers a significant improvement to the calculation efficiency.

3. Bridge deck example

To investigate the capability of DIVEX for the analysis of the flow field around a representative geometry, a study of the Great Belt East Suspension bridge has been undertaken. The Great Belt East bridge with a main span of 1624 m, opened in June 1998, and forms one of the longest single spans in the world. The bridge forms part of the link between the islands of Funen and Zealand in Denmark (Larsen *et al*. 1992 and 1993). The basic profile and structural properties of the main span section are given in Fig. 1. All of the analyses presented herein are performed on the main suspended span in a smooth flow field at a Reynolds number of 10^5. For the static and flutter computations the time step $\Delta tU/B = 0.005$ is employed along with a first order Euler scheme for vortex particle convection. The main deck is discretised using 144 panels, with 7 vortices per panel. Vortex core radius and creation distance are $0.001B$ and $0.0005B$ respectively.

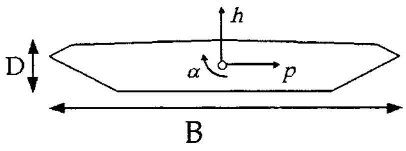

Property	
Deck width: B (m)	31.0
Deck Height: D (m)	4.4
Mass: m (Kg/m)	22.74×10^{3}
Inertia: I (Kgm^2/m)	2.47×10^{6}
Vertical freq. : f_h (Hz)	0.099
Torsional freq. : f_α (Hz)	0.272
Along wind freq: f_p (Hz)	0.052
Damping ratio : ζ	0.002

Fig. 1 Basic dimensions and properties of the Great Belt East Bridge

3.1. Summary of static results

A series of calculations on the static section were performed at a range of angles of incidence from -10° to +10°. Most modern long span suspension bridge designs, as in this case, utilise a streamlined box section to ensure that the increase in the force coefficients with incidence is not so dramatic to produce a fundamentally unstable design.

In the 0° case, the flow over the bridge deck is virtually fully attached along the top and bottom surfaces, with the main separation zone stemming from the rear top and bottom corners, as illustrated in Fig. 2. The prime reason for this is the streamlined profile in conjunction with the simplified geometric model employed, which omits more complex features such as crash barriers and cable supports that would disturb the flow.

The static force coefficients for the section are presented in Figs. 3 and 4, compared with experimental results from a section model test (Reinhold *et al.* 1992) and also with results from a finite difference grid based numerical method (Kuroda 1997). The wind tunnel tests were performed with a free stream turbulence intensity of 6.5-7%. C_L and C_M are non-dimensionalised with respect to the along wind body dimensions, B and B^2, whereas C_D is non-dimensionalised using the crosswind dimension, D.

The results presented by Kuroda (1997) also use a simplified deck section with the barriers omitted. Results at 0° incidence are also presented in Table 1 along with other vortex method results on the Great Belt section (Walther 1994 and Larsen *et al.* 1997a and 1997b), where again a simplified model geometry was employed. In general the results compare well with the experiment, in particular C_L and C_M , and show favourable comparison with the alternative numerical methods.

The model predictions for C_D at 0° are low when compared to experiment, a feature which reflects

Fig. 2 Predicted flow field around Great Belt East main suspended section at 0° incidence

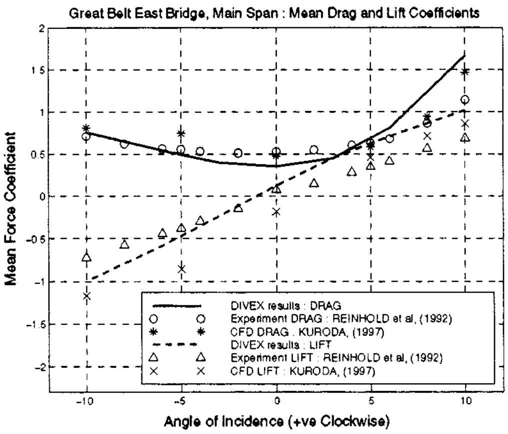

Fig. 3 Variation of mean lift and drag coefficients with angle of incidence

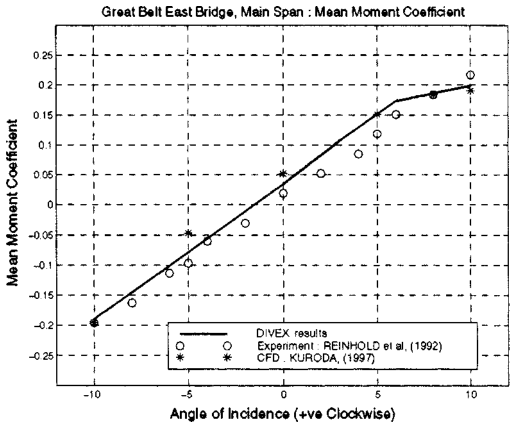

Fig. 4 Variation of mean moment coefficient with angle of incidence

Table 1 Comparison of experimental and calculated static force coefficients for Great Belt East main suspended span

Results	C_D ($\alpha = 0°$) -	C_L ($\alpha = 0°$) -	$dC_L/d\alpha$ ($\alpha = 0°$) rad^{-1}	C_M ($\alpha = 0°$) -	$dC_M / d\alpha$ ($\alpha = 0°$) rad^{-1}	St ($\alpha = 0°$)
Experiment (Reinhold *et al.* 1992)	0.57	0.067	4.37	0.028	1.17	0.12-0.14
DIVEX	0.3544	0.127	6.58	0.0519	1.34	0.13-0.16
Finite difference (Kuroda 1997)	0.4811	-0.1792	7.567	0.0345	1.135	0.163
Vortex Method (Larsen *et al.* 1997a and 1997b)	0.430	0.000	4.13	0.027	1.15	0.168

the lack of modelling of the crash barriers and parapets in the calculations (Larsen *et al.* 1997b), elements that were included in the wind tunnel model. The Strouhal number obtained from the DIVEX results ($\Delta tU / B = 0.02$) are very close to the experiment. A range is given because the power spectrum of the lift data exhibits a broad band response, as indicated in Fig. 5. Although the spectrum in smooth flow might be expected to be narrow band, the slenderness of the deck reduces the coherence of the vortex wake and hence increases the bandwidth.

3.2. Aerodynamic derivatives with/without added vanes

On flexible long span bridges coupled degree of freedom flutter is often encountered and careful design of the section is essential to ensure that the critical flutter velocity is within the relevant design criteria. For small amplitude oscillations, the unsteady aerodynamic load coefficients may be treated as linear in the structural displacements and their first derivatives. In the first phase of this work, DIVEX has been employed purely in aerodynamic mode to produce a set of force time histories obtained from a series of tests with the deck undergoing prescribed harmonic motions for the individual degrees of freedom. In theory, it is possible to extract eighteen derivatives from such tests (H_i^*, P_i^* and A_i^*, i = 1-6) as defined below (Jain *et al.* 1996)

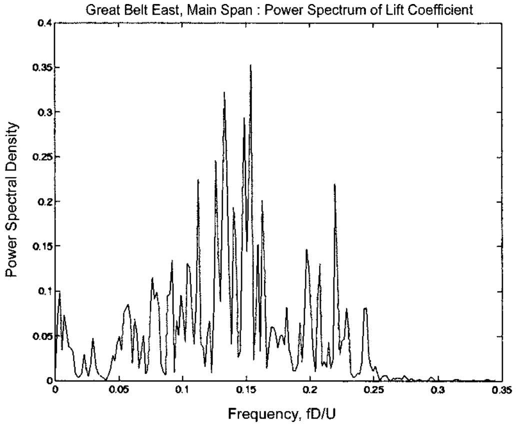

Fig. 5 Power Spectrum of lift coefficient at zero degrees incidence

$$L_h = \frac{1}{2}\rho U^2(2B)\left[KH_1^*(K)\frac{\dot{h}}{U} + KH_2^*(K)\frac{B\dot{\alpha}}{U} + K^2H_3^*(K)\alpha + K^2H_4^*(K)\frac{h}{B} + KH_5^*(K)\frac{\dot{p}}{U} + K^2H_6^*(K)\frac{p}{B}\right]$$

$$D_p = \frac{1}{2}\rho U^2(2B)\left[KP_1^*(K)\frac{\dot{p}}{U} + KP_2^*(K)\frac{B\dot{\alpha}}{U} + K^2P_3^*(K)\alpha + K^2P_4^*(K)\frac{p}{B} + KP_5^*(K)\frac{\dot{h}}{U} + K^2P_6^*(K)\frac{h}{B}\right]$$

$$M_\alpha = \frac{1}{2}\rho U^2(2B^2)\left[KA_1^*(K)\frac{\dot{h}}{U} + KA_2^*(K)\frac{B\dot{\alpha}}{U} + K^2A_3^*(K)\alpha + K^2A_4^*(K)\frac{h}{B} + KA_5^*(K)\frac{\dot{p}}{U} + K^2A_6^*(K)\frac{p}{B}\right]$$

which can be used to estimate flutter onset speeds given the structural data. Traditionally, the most important influence on flutter characteristics have been the A_i^* and H_i^* derivatives, associated with coupled transverse and torsional motion. In the present work the derivatives associated with the lift and moment only are presented, although future studies will investigate the influence of along wind derivatives. The derivatives for the deck in isolation are illustrated in Figs. 6 and 7, compared with the experimentally obtained counterparts (Reinhold *et al.* 1992). The wind tunnel tests were carried out in smooth flow (0.5% turbulence intensity).

The resulting flutter speeds obtained from selected derivative sets are indicated in Table 2, in which the experimentally derived data of Reinhold *et al.* (1992) are also included. The value associated with the inclusion of *P* derivatives provides an assessment based on the quasi steady expressions for P_1-P_3 (Singh *et al.* 1996).

An interesting point to note with the Great Belt flutter derivatives is that A_2^* does not exhibit the change in sign that is characteristic for 1DOF torsional flutter. The derivative A_2^* represents the aerodynamic damping in the torsional direction and the “negative damping” criteria necessary for torsional flutter only occurs at positive A_2^*. Hence, as A_2^* remains negative over the whole range of reduced velocity, the flutter oscillation for this section is a 2DOF coupled flutter in both the vertical and torsional directions. From Table 2 it can be seen that the along wind component is not involved in this aeroelastic instability.

For streamlined sections such as that of the Great Belt East bridge, the critical flutter velocity may be increased by the addition of guide vanes that act as flow control devices. Such devices have been studied by Cobo Del Arco *et al.* (1997), Kobayashi *et al.* (1992) and Ostenfeld *et al.* (1992)

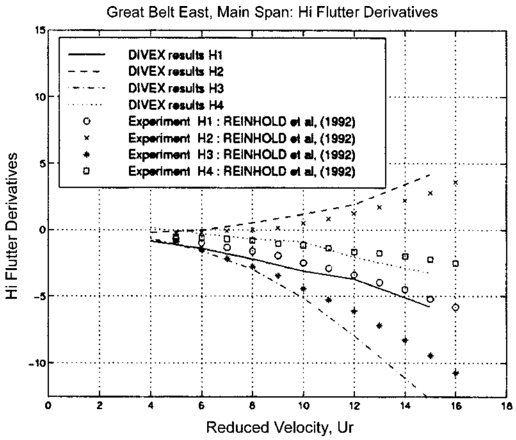

Fig. 6 H_i^* derivatives for Great Belt East main span

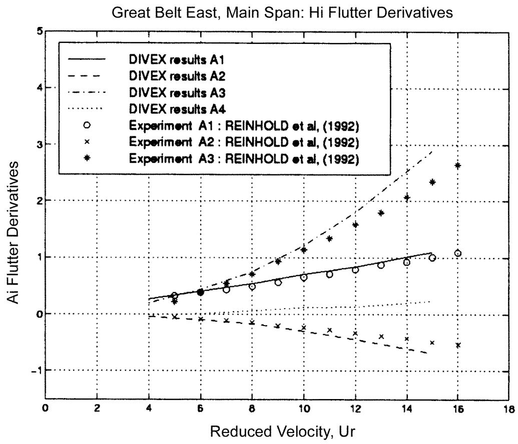

Fig. 7 A_i^* derivatives for Great Belt East main span

Table 2 Flutter velocities for Great Belt East Main Span

Derivatives	Critical Velocity , U_c (m/s)
H_i , A_i (i = 1-3)	74.9
H_i , A_i (i = 1-4)	71.9
H_i , A_i (i = 1-4), P_1-P_3 (qs)	71.9
Experiment	70-75

indicating the effects of both passive and actively controlled devices. It is essential that the guide vanes be located far enough from the bridge deck as is practical to ensure operation outside of the bridge shear layers. Typically the vanes have a chord length that is around 10% of the deck section width.

A brief study into the effect of passive and active control vanes on the flutter stability has been carried out using the DIVEX code. As part of the study, various configurations of passive and active control vanes have been applied to the Great Belt East main suspended span to investigate their effect on the flutter criteria (Fig. 8). As this is only a study of the effect of the vanes, a basic elliptical cross section is used. Each of the vanes has chord length 10% of the bridge section width. The effect on the flutter velocity of passive vanes at different angles, and of active vanes at different phase angles, were studied. In the calculations, the bridge was given a forced sinusoidal oscillation in either the transverse or torsional DOF and for the passive calculations, the vanes were oscillated in phase with the bridge and with the same amplitude and frequency. To demonstrate the active vanes, the control surfaces were given a forced motion that simulates the displacements that would be activated by the controller when the bridge is oscillating in the torsional DOF. The prescribed displacements of the vanes are illustrated in Fig. 9 for a phase angle $\phi = 60^{\circ}$.

Varying performance of the flow control vanes can be achieved by using different values for the amplitude factor, M, and the phase relative to the bridge section, ϕ. In each calculation, the downstream vane is in opposite phase to the upstream vane. Five different configurations of guide vanes were used, two of which were passive, where the vanes are effectively rigidly fixed to the bridge section, and three using active vanes, each with different phase angles as summarised below :

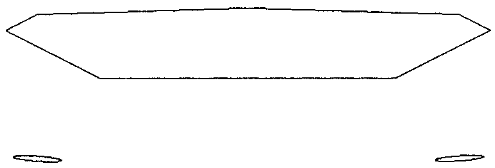

Fig. 8 Great Belt East main suspended section with flow control vanes - DIVEX model

Bridge torsional motion : $\alpha(t) = \alpha_0 \sin\left(\frac{2\pi t}{U_r}\right)$

Vane motion : $\alpha_v(t) = M\alpha_0 sin\left(\frac{2\pi t}{U_r} + \phi\right)$

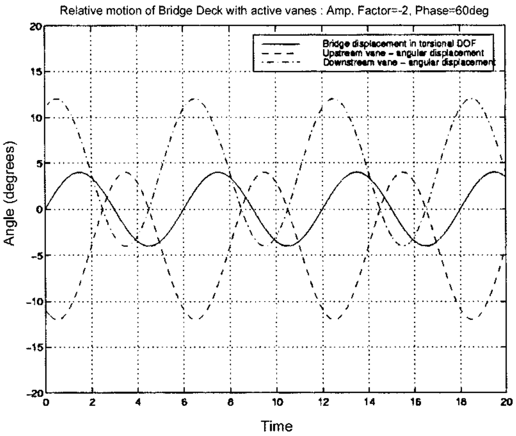

Fig. 9 Prescribed motion of active vanes

(1) Passive vanes : $\alpha = 0^o$
(2) Passive vanes : $\alpha = 4^o$
(3) Active vanes : $M = 2$, $\phi = 0^o$
(4) Active vanes : $M = 2$, $\phi = 60^o$
(5) Active vanes : $M = 2$, $\phi = 90^o$

The flutter derivatives are relatively unaffected by the vanes, with the exception of H_2^* and A_2^* for the active vanes with $\phi = 60^o$ and $\phi = 90^o$, as illustrated in Figs. 10 and 11. The flutter velocity for each configuration is calculated using the structural properties given in Fig. 1 using the assumption that the addition of the vanes have no effect on the mass and stiffness of the structure. This assumption may be a little unrealistic but allows an investigation of how the aerodynamic properties of the bridge are affected by the flow control devices. The results are given in Table 3.

As expected, the passive guide vanes do not have a large effect on the critical flutter velocity and in fact very slightly reduce the stability of the bridge. This result agrees with the findings of the studies in Ostenfeld *et al.* (1992) and Kobayashi *et al.* (1992). For the active vanes the $\phi = 0^o$ case gives a slightly lower flutter speed than the bridge deck without vanes. The flow control vanes can improve the aeroelastic stability by effectively increasing the aerodynamic damping. The A_2^* derivative is the damping coefficient and the H_2^* derivative is the coupling damping coefficient for torsional motion. It is clear that the changes in magnitude of these two derivatives in particular affects the aerodynamic damping of the structure and hence the critical flutter velocity.

The reduction in flutter velocity for the $\phi = 0^o$ case is to be expected from the results of Kobayashi *et al.* (1992). The two cases where $\phi > 0^o$ show a significant change in the flutter velocity, and in the $\phi = 90^o$ calculation, no flutter velocity was found even when the aerodynamic

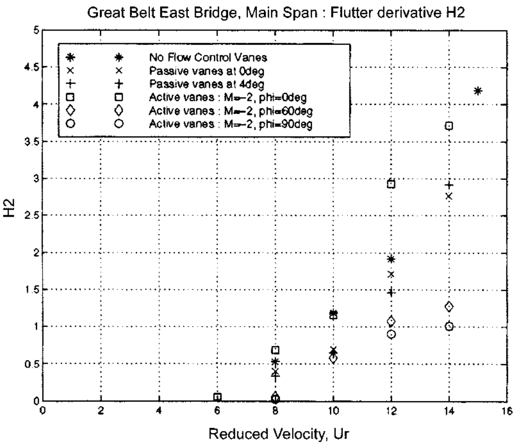

Fig. 10 H_2^* derivatives for the Great Belt East main span with flow control vanes

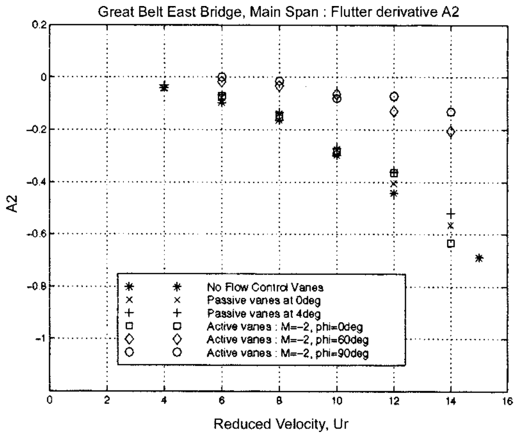

Fig. 11 A_2^* derivatives for Great Belt East main span

Table 3 Effect of passive control vanes on critical flutter velocity

Configuration	Critical Velocity, U_c (m/s)
No vanes	71.6
Passive vanes: $\alpha = 0^{\circ}$	68.2
Passive vanes: $\alpha = 4^{\circ}$	70.9
Active vanes: $\phi = 0^{\circ}$	65.5
Active vanes: $\phi = 60^{\circ}$	108.1
Active vanes: $\phi = 90^{\circ}$	Not found in range

derivatives were extrapolated beyond the range of reduced velocities used in the calculations. Again, this agrees with the other studies from which it was found that, as M increases, the flutter velocity tends to infinity for a phase of 90°, or even less at the higher amplitude factors. For $\phi = 60°$, the flutter velocity has been increased by approximately 51% in agreement with the previous studies.

3.3. Full aeroelastic solution

A dynamic solver has been implemented in the DIVEX code for the calculation of the time-dependent aeroelastic response of 2-D bluff bodies, including bridge decks. The equations governing the fluid-structure interaction are cast, for convenience, in first order form using non-dimensional variables. For coupled vertical and torsional motion these are:

$$\begin{bmatrix} \eta \\ \eta' \\ \alpha \\ \alpha' \end{bmatrix}' = \begin{bmatrix} 0 & 1 & 0 & 0 \\ -K_h^2 & -2K_h\zeta_h & 0 & 0 \\ 0 & 0 & 0 & 1 \\ 0 & 0 & -K_\alpha^2 & -2K_\alpha\zeta_\alpha \end{bmatrix} \begin{bmatrix} \eta \\ \eta' \\ \alpha \\ \alpha' \end{bmatrix} + \begin{bmatrix} 0 \\ C_L/m_r \\ 0 \\ C_M/I_r \end{bmatrix}$$

where $\eta = h / B$, $(\ )' = (B / U)\,(d / dt)$, K is reduced frequency, m_r and I_r are reduced mass and inertia

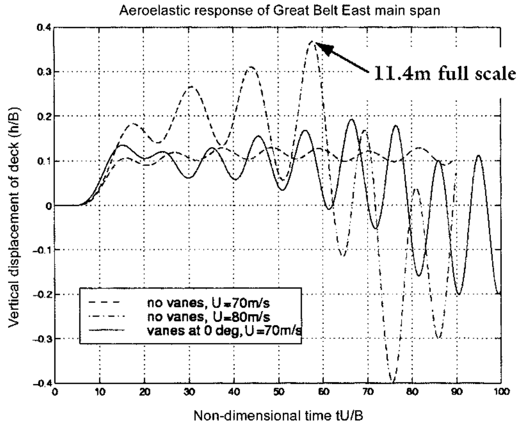

Fig. 12 Vertical response of the Great Belt East main span with and without vanes

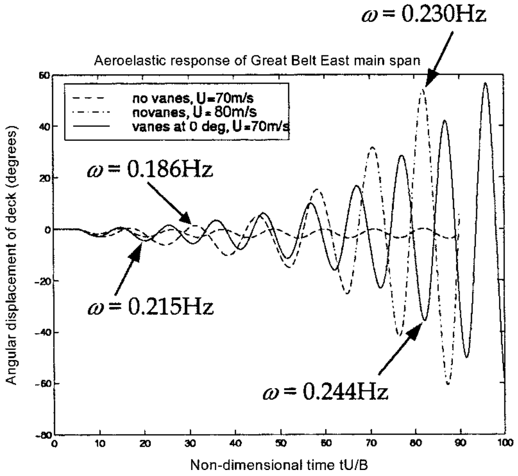

Fig. 13 Torsional response of the Great Belt East main span with and without vanes

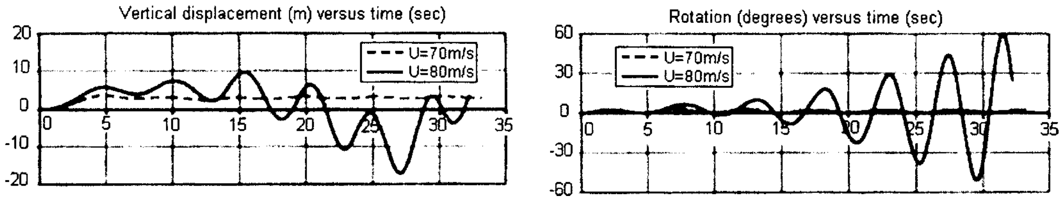

Fig. 14 FSI simulation of flow over Great Belt East (Enevoldsen *et al.* 1999)

parameters.

The equations are integrated forward in time using the following fourth order Runge-Kutta scheme:

For system $\boldsymbol{y}' = \boldsymbol{A}\boldsymbol{y} + \boldsymbol{B}$

$$\boldsymbol{k}_1 = \Delta t\boldsymbol{y}'(\boldsymbol{y}^t)$$

$$\boldsymbol{k}_i = \Delta t\boldsymbol{y}'\left(\boldsymbol{y}^t + \frac{1}{2}\boldsymbol{k}_{i-1}\right) \qquad \text{for } i = 2, 3$$

$$\boldsymbol{k}_4 = \Delta t\boldsymbol{y}'(\boldsymbol{y}^t + \boldsymbol{k}_3)$$

$$\boldsymbol{y}^{t+\Delta t} = \boldsymbol{y}^t + \frac{\boldsymbol{k}_1}{6} + \frac{\boldsymbol{k}_2}{3} + \frac{\boldsymbol{k}_3}{3} + \frac{\boldsymbol{k}_4}{6} + O(\Delta t^5)$$

This scheme was employed to provide confirmation of the previous flutter onset predictions for the Great Belt East bridge. In particular, calculations have been performed for the deck in isolation at $U = 70$ m/s and $U = 80$ m/s, and for the case with passive vanes set at 0° to the main deck at $U = 70$ m/s. The results are illustrated in Figs. 12 and 13, which illustrate the vertical and torsional response for each configuration. As expected the isolated deck is stable at 70 m/s, but unstable at 80 m/s, and the pattern of the developing instability is very similar to that predicted by Enevoldsen *et al.* (1999), shown in Fig. 14.

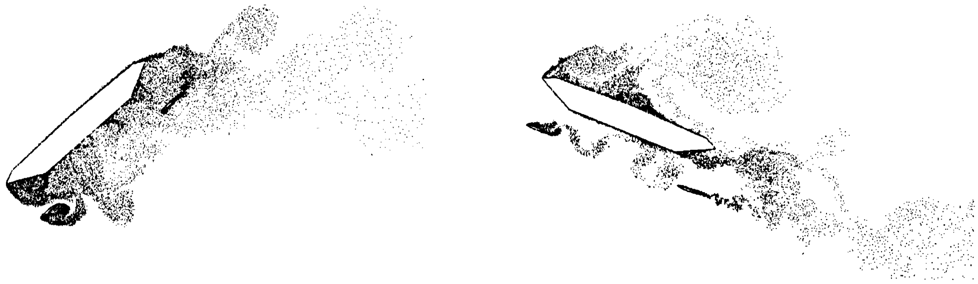

Fig. 15 Stills of the developing flutter instability of the Great Belt East main span with vanes at 0^0, U = 70 m/s

Note that torsion is dominant in this case with the oscillating frequency in between the vertical and torsional natural frequencies, but driven very close to the latter, more so as the instability develops. Snapshots from the growing instability of the deck with vanes arrangement are illustrated in Fig. 15.

4. Conclusions

A Discrete Vortex Method (DIVEX) has been developed at the Department of Aerospace Engineering, University of Glasgow. A variety of test cases in the fields of aeronautics and wind engineering have been studied. DIVEX has been applied to static and oscillating bridge deck sections. The calculated flutter derivatives from oscillatory calculations are in good agreement with experiment and also compare favourably with other computational methods. These derivatives have been used to give an accurate prediction of the critical flutter velocity of the bridge section examined. The effect of active and passive flow control devices on the structural stability of the bridge deck have also been investigated and the dependency of flutter velocity on the phase of the vane motion are in agreement with previous experimental and analytical studies. The results illustrate the potential of the DIVEX code as a design tool for single and multiple body configurations, where aeroelastic assessment can be based on the extraction of derivatives and/or the prediction of full aeroelastic response. Among future intended projects is a more detailed investigation into the influence of along wind derivatives on the critical flutter speed of bridge decks.

References

Billah, K.Y. and Scanlan, R.H. (1991), “Resonance, Tacoma Narrows Bridge failure, and undergraduate physics textbooks”, *American J. of Phys.* **59**(2), 118-124.

Carrier, J., Greengard, L. and Rokhlin, V. (1988), “A fast adaptive multipole algorithm for particle simulations”, *SIAM J. Sci. Stat. Comp.* **9**, 669-686.

Chorin, A.J. (1973), “Numerical study of slightly viscous flow”, *J. Fluid Mech.* **57**, 785-796.

Cobo del Arco, D. and Bengoechea, A.C.A. (1997), “Some proposals to improve the wind stability performance of long span bridges”, *Proc. 2nd European and African Conf. Wind Eng.*, Genova, Italy, 22-26 June 1997, 1577-1584.

Enevoldsen, I., Pedersen, C., Hansen, S.O., Thorbek, L.T. and Kvamsdal, T.K. (1999), “Computational wind simulations for cable-supported bridges”, *Proc. 10th Int. Conf. on Wind Eng.*, Copenhagen, Denmark, 1999.

Huston, D.R., Bosch, H.R. and Scanlan, R.H. (1988), “The effects of fairings and of turbulence on the flutter derivatives of a notably unstable bridge deck”, *J. Wind Eng. Ind. Aerod.* **29**(1-3), 339-349.

Jain, A., Jones, N.P. and Scanlan, R.H. (1996), “Coupled aeroelastic and aerodynamic response analysis of long-span bridges”, *J. Wind Eng. Ind. Aerod.* **60**, 69-80.

Kobayashi, H. and Nagaoka, H. (1992), “Active control of flutter of a suspension bridge”, *J. Wind Eng. Ind. Aerod.* **41-44**, 143-151.

Kuroda, S. (1997), “Numerical simulation of flow around a box girder of a long span suspension bridge”, *J. Wind Eng. Ind. Aerod.* **67-68**, 239-252.

Kwon, S. and D Chang, Y. “Active suppression of flutter and gust response of bridge using edge control surfaces”, *Proc. 10th Int. Conf. on Wind Eng.*, Copenhagen, Denmark, 1999.

Larsen, A. and Gimseng, N.J. (1992), “Wind engineering aspects of the East Bridge tender project”, *J. Wind Eng. Ind. Aerod.* **41-44**, 1405-1416.

Larsen, A. (1993), “Aerodynamic aspects of the final design of the 1624m suspension bridge across the Great Belt”, *J. Wind Eng. Ind. Aerod.* **48**, 261-285.

Larsen, A. (1997a), “Advances in aeroelastic analysis of suspension and cable-stayed bridges”, *Proc. 2nd European and African Conf. Wind Eng.*, Genova, Italy, 22-26 June 1997, 61-75.

Larsen, A. and Walther, J.H. (1997b), “Aeroelastic analysis of bridge girder sections based on discrete vortex simulations”, *J. Wind Eng. Ind. Aerod.* **67-68**, 253-265.

Leonard, A. (1980), “Vortex methods for flow simulation”, *J. Comp. Phys.* **37**, 289-335.

Lin, H. and Vezza, M. (1996), “A pure vortex method for simulating unsteady, incompressible, separated flows around static and pitching aerofoils”, *Proc. 20th ICAS Conf.*, Sorrento, Italy, 8-13 September 1996, 2184-2193.

Lin, H., Vezza, M. and Galbraith, R.A.McD. (1997a), “Discrete vortex method for simulating unsteady flow around pitching aerofoils”, *AIAA J.* **35**(3), 494-499.

Lin, H. (1997b), “Prediction of separated flows around pitching aerofoils using a discrete vortex method”, Ph.D. Thesis, Dept. of Aerospace Engineering, University of Glasgow, Scotland, UK.

Nagao, F., Utsunomiya, H., Oryu, T. and Manabe, S. (1993), “Aerodynamic efficiency of triangular fairing on box girder bridge”, *J. Wind Eng. Ind. Aerod.* **49**, 565-574.

Omenzetter, P., Wilde, K. and Fujino, Y. (1999), “Flutter suppression in long span bridges by a passive bridge deck-flaps control system”, *Proc. 10th Int. Conf. on Wind Eng.*, Copenhagen, Denmark.

Ostenfeld, K.H. and Larsen, A. (1992), “Bridge engineering and aerodynamics”, Aerodyn. Large Bridges, ed. A. Larsen, *Proc. 1st Int. Symp., Copenhagen*, Denmark, 19-21 February 1992, 3-22.

Perlman, M. (1985), “On the accuracy of vortex methods”, *J. Comp. Phys.* **59**, 200-223.

Puckett, E.G. (1993), “Vortex methods : an introduction and survey of selected research topics”, *Incompressible Computational Fluid Dynamics*, (ed. M.D. Gunzburger and R.A. Nicolaides), Cambridge University Press: 335-407.

Reinhold, T.A., Brinch, M. and Damsgaard, A. (1992), “Wind tunnel tests for the Great Belt link”, Aerodyn. Large Bridges, ed. A. Larsen, *Proc. 1st Int. Symp., Copenhagen*, Denmark, 19-21 February 1992, 255-267.

Sarpkaya, T. (1989), “Computational methods with vortices - the 1988 Freeman Scholar lecture”, *J. Fluids Eng.*, **111**, 5-52.

Scanlan, R.H. and Tomko, J.J. (1971), “Airfoil and bridge deck flutter derivatives”, *J. Eng. Mech. Div.*, ASCE. **97**, 1717-1737.

Scanlan, R.H. (1992), “Wind dynamics of long-span bridges”, Aerodyn. Large Bridges, ed. A. Larsen, *Proc. 1st Int. Symp., Copenhagen*, Denmark, 19-21 February 1992, 47-57.

Scanlan, R.H. (1997), “Some observations on the state of bluff-body aeroelasticity”, *J. Wind Eng. Ind. Aerod.* **69-71**, 77-90.

Singh, L., Jones, N.P., Scanlan, R.H. and Lorendeaux, O. (1996), “Identification of lateral flutter derivatives of bridge decks”, *J. Wind Eng. Ind. Aerod.* **60**, 81-89.

Spalart, P.R. (1988), “Vortex methods for separated flows”, *NASA TM 100068*.

Taylor, I.J. and Vezza, M. (1998), “Computation of unsteady wind loading on bluff bodies using a discrete vortex method”, *Proc. 2nd East Euro. Conf. Wind Eng.*, Prague, Czech Republic, 7-11 September 1998, 127-134.

Taylor, I.J. (1999), “Study of bluff body flow fields and aeroelastic stability using a discrete vortex method”, Ph.D. Thesis, Dept. of Aerospace Engineering, University of Glasgow, Scotland, UK.

Walther, J.H. (1994), “Discrete vortex method for two-dimensional flow past bodies of arbitrary shape undergoing prescribed rotary and translational motion”, AFM-94-11, Ph.D. Thesis, Department of Fluid Mechanics, Technical University of Denmark.